PTEP

Prog. Theor. Exp. Phys. **2025** 053D02 (11 pages)
DOI: 10.1093/ptep/ptaf051

Discovery of ^{98}Sn Produced by the Projectile Fragmentation of a 345-MeV/Nucleon ^{124}Xe Beam

H. Suzuki[1,*], N. Fukuda[1], H. Takeda[1], Y. Shimizu[1], D. S. Ahn[1,2], T. Komatsubara[1], A. Algora[3,4], B. Rubio[3], J. A. Victoria[3], J. L. Tain[3], A. Tolosa[3], J. Agramunt[3], E. Nacher[3], S. E. A. Orrigo[3], V. Guadilla[5,6], G. Kiss[4], D. Sohler[4], I. Kuti[4], T. Davinson[7], O. B. Hall[7], D. Kahl[7,8], C. G. Bruno[7], C. J. Appleton[7], P. J. Woods[7], S. Nishimura[1], H. Baba[1], D. Nishimura[1], T. Isobe[1], M. Kaneko[1], S. Kubono[1], H. Sakurai[1], H. Shimizu[1], T. Sumikama[1], P. Doornenbal[1], M. L. Cortes[9], Zs. Podolyak[10], E. Ganioglu[11], Y. Fujita[12], F. Molina[13], J. Liu[14,15], J. Lee[14], K. P. Rykaczewski[16], M. Wolinska-Cichocka[17], M. Labiche[18], C. J. Griffin[19], S. Bae[20], J. Ha[20], Yu. A. Litvinov[21], K. Kusaka[1], Y. Yanagisawa[1], M. Ohtake[1], N. Fukunishi[1], and S. Michimasa[1]

[1]*RIKEN Nishina Center for Accelerator-Based Science, RIKEN, 2-1 Hirosawa, Wako, Saitama 351-0198, Japan*
[2]*Center for Exotic Nuclear Studies, Institute for Basic Science, 55 Expo-ro, Doryong, Yuseong-gu, Daejeon 34126, Republic of Korea*
[3]*Instituto de Física Corpuscular, CSIC-Universitat de València, Parc Científic de la Universitat de València, Cl Catedrático José Beltrán, 2, E-46980 Paterna, Spain*
[4]*HUN-REN, Institute for Nuclear Research (ATOMKI), P.O. Box 51, 4001 Debrecen, Hungary*
[5]*SUBATECH, IMT Atlantique, Université de Nantes, 4, rue Alfred Kastler, 44307 Nantes, France*
[6]*Faculty of Physics, University of Warsaw, ul. Pasteura 5, 02-093 Warszawa, Poland*
[7]*School of Physics and Astronomy, The University of Edinburgh, James Clerk Maxwell Building, Peter Guthrie Tait Road, Edinburgh EH9 3FD, UK*
[8]*Facility for Rare Isotope Beams, Michigan State University, 640 South Shaw Lane, East Lansing, MI 48824, USA*
[9]*Instituto Nazionale di Fisica Nucleare, Laboratori Nazionali di Legnaro, Viale dell'Università, 2-35020 Legnaro, Italy*
[10]*Department of Physics, University of Surrey, Guildford, Surrey GU2 7XH, UK*
[11]*Department of Physics, Istanbul University, PK:34134 Vezneciler, Istanbul, Turkey*
[12]*Department of Physics, University of Osaka, 1-1 Machikaneyama, Toyonaka, Osaka 560-0043, Japan*
[13]*Comisión Chilena de Energía Nuclear, Amunátegui 95, 8340701 Santiago, Región Metropolitana, Chile*
[14]*Department of Physics, University of Hong Kong, Chong Yuet Ming Physics Building, University of Hong Kong, Pokfulam Road, Hong Kong*
[15]*CAS Key Laboratory of High Precision Nuclear Spectroscopy, Instutute of Modern Physics, Chinese Academy of Sciences, 509 Nanchang Rd., Lanzhou 730000, China*
[16]*Physics Division, Oak Ridge National Laboratory, 1 Bethel Valley Road, Oak Ridge, TN 37830, USA*
[17]*Heavy Ion Laboratory, University of Warsaw, ul. Pasteura 5A 02-093 Warszawa, Poland*
[18]*Daresbury Laboratory, Science and Technology Facilities Council, Keckwick Lane, Daresbury, WA4 4AD, UK*
[19]*TRIUMF, 4004 Wesbrook Mall, Vancouver, British Columbia V6T 2A3, Canada*
[20]*Department of Physics and Astronomy, Seoul National University, 1 Gwanak-ro, Gwanak-gu, Seoul 08826, Republic of Korea*
[21]*GSI Helmholtzzentrum für Schwerionenforschung GmbH, Planckstraße 1 64291 Darmstadt, Germany*

*hsuzuki@ribf.riken.jp

Received December 26, 2024; Revised March 6, 2025; Accepted April 6, 2025; Published April 7, 2025

We present the discovery of a new isotope of ^{98}Sn beyond the double-magic $N = Z = 50$ nucleus ^{100}Sn. ^{98}Sn was identified among the projectile-fragmentation products of a ^{124}Xe beam at 345 MeV/nucleon at the RI Beam Factory, RIKEN, Japan. Additionally, we have confirmed the production of ^{96}In and ^{94}Cd, previously reported as new isotopes at RIKEN. These highly proton-rich nuclei were separated and identified using the large-acceptance two-stage separator BigRIPS. Furthermore, we have determined the cross sections of ^{98}Sn and its neighboring nuclei. These experimental values were compared to the semi-empirical cross-section formula EPAX3.1a, resulting in a reduction of the predicted cross sections by roughly a factor of 5.

Subject Index D23

1. Introduction

Self-conjugate nuclei, isotopes consisting of the same number of protons (Z) and neutrons (N), and neighboring species have attracted considerable interest regarding their nuclear mirror symmetry and the astrophysical *rp*-process. Recently, some cases of mirror-symmetry violation have been found; e.g. the spin parities of the ground states of ^{73}Sr and ^{73}Br are suggested to be different, $5/2^-$ and $1/2^-$, respectively [1]. Another example is the shape changes in ^{70}Kr and ^{70}Se; the former is prolate and the latter is spherical [2]. ^{100}Sn is presently the heaviest bound $N = Z$ doubly-magic nuclide, and its structure and reactions are actively investigated both experimentally and theoretically [3–8]. Its vicinity is considered to be a possible end point of the *rp*-process [9,10], although through compositional inertia [11] nucleosynthesis is known to proceed to ^{126}Xe [12], and undiscovered isotopes such as ^{98}Sn were not included in the "closed" SnSbTe cycle [9]. Therefore, it is fundamental information to understand not only the $g_{9/2}$-shell structure but also the nucleosynthesis in the proton-rich region in which isotopes are so stable and how long they can exist.

The proton dripline around the ^{100}Sn region has been established only partly in experiments. At $Z = 41$, 43, 45, and 47, the driplines are considered to be reached already by the short half-lives (< 100 ns) of ^{81}Nb, ^{85}Tc, ^{89}Rh, and ^{93}Ag [6,13,14]. The proton separation energies of $^{105}_{51}$Sb, $^{109}_{53}$I, and $^{114}_{55}$Cs [15] reveal that they are located beyond the dripline. On the other hand, it is not known yet whether the driplines at $_{49}$In and even-Z isotopes are reached or not. According to the mass models [15–27], currently, the driplines in odd-Z isotopes have been reached, and the ones in even-Z are partly reached. Discovery of new isotopes and study of nuclear boundness provides strong constraints to the mass models.

Since the RI Beam Factory (RIBF) [28] at RIKEN began operations in 2007, various new isotopes have been produced [29,30]. We have discovered 173 new isotopes in total: 147 [31–37], 10 [6,14,38,39], 4 [40,41], 11 [42,43], and 1 [44] new isotopes produced from the 345-MeV/nucleon ^{238}U, ^{124}Xe, ^{78}Kr, ^{70}Zn, and ^{48}Ca primary beams, respectively. In this study, we focused on the proton-rich region around ^{100}Sn using the ^{124}Xe beam.

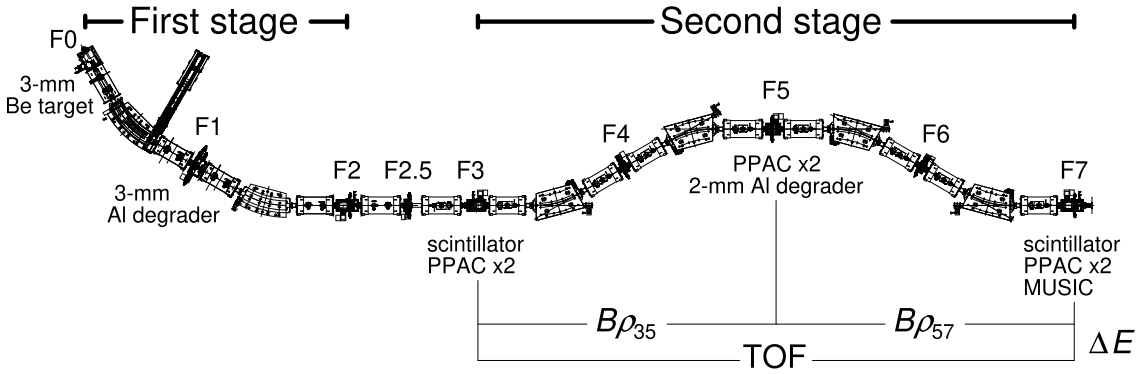

Fig. 1. Layout of the BigRIPS separator. Labels Fn except F2.5 indicate the focal planes. At F2.5, the ion optics is designed such that the beam is parallel. The first and second stages span from F0 to F2 and from F3 to F7, respectively. F2, F3, and F7 are fully achromatic focal planes, whereas F1 and F5 are momentum-dispersive ones. The production target at F0, the energy degraders at F1 and F5, and the PID detectors at F3, F5, and F7 are shown. The measurement schemes for the time of flight (TOF), magnetic rigidities ($B\rho_{35}$ and $B\rho_{57}$), and energy loss (ΔE) are also included. MUSIC, multisampling ionization chamber; PPAC, parallel plate avalanche counter.

We also present information on the production cross sections of proton-rich radioactive isotopes (RI) around ^{100}Sn. They are essential information to understand the production mechanism of RI beams based on the framework of a two-step process model: Abrasion + Ablation processes [45]. Recently, excitation energy of pre-fragments was discussed with the cross sections in the ^{78}Kr + Be reactions [46] based on the Abrasion-Ablation model [47] to understand the RI-beam production mechanism. The cross-section data in the ^{124}Xe + Be reaction obtained in our study also contribute to revealing the production mechanism in the medium-heavy region.

2. Experiment

Highly proton-rich RI beams around ^{100}Sn were produced from a 345-MeV/nucleon $^{124}Xe^{52+}$ beam impinging on a 3-mm ^{9}Be production target located at the F0 focal plane, the entrance of the BigRIPS separator [48–50]. The experimental setup of BigRIPS is shown in Fig. 1 along with the production target, energy degraders, and particle-identification (PID) detectors. The RIs of interest were separated at the first stage (F0–F2) of BigRIPS by the $B\rho$-ΔE-$B\rho$ method [51,52] using a 3-mm Al wedge degrader located at the F1 dispersive focal plane. The intensity of the primary beam was monitored using 3-fold plastic scintillators [53] counting light charged particles scattered from the Be target. The typical intensity of the ^{124}Xe beam used was 110–120 particle nA (pnA).

The second stage spans from F3 to F7 and it is for the PID and further particle separation. The PID detectors consisted of 0.2-mm plastic scintillators at F3 and F7, position-sensitive parallel plate avalanche counters (PPACs) [54] at F3, F5, and F7, and a multisampling ionization chamber (MUSIC) [55,56] filled with P-10 gas (90% Ar + 10% CH_4) at F7. The mass-to-charge ratios (A/q) and atomic numbers (Z) of the particles were obtained using the TOF-$B\rho$-ΔE method (TOF: time of flight; $B\rho$: magnetic rigidity; ΔE: energy loss) [57]. The TOF was measured using the plastic scintillators; the $B\rho$ values were calculated from the positions and angles measured by the PPACs at each focal plane using the trajectory-reconstruction technique [57]; and ΔE was measured using the MUSIC. The PID plots were calibrated by the isomer-tagging

Table 1. Experimental settings used for the discovery of ^{98}Sn produced by the ^{124}Xe + Be reaction at 345 MeV/nucleon.

	Setting 1	Setting 2
Primary beam	345-MeV/nucleon ^{124}Xe	
Central particle	$^{100}Sn^{50+}$	
F0 target (Be)	3 mm (effective thickness; 3.051 mm)	
F1 degrader (Al)	3 mm (effective thickness; 2.843 mm)	
F5 degrader (Al)	2 mm (effective thickness; 1.974 mm)	
$B\rho$ at F0–F1 (Tm)	5.320	
$B\rho$ at F1–F2 (Tm)	4.725	
$B\rho$ at F3–F5 (Tm)	4.662	
$B\rho$ at F5–F7 (Tm)	4.114	
Exit beam dump (mm)	±125	±125
F1 slits (mm)	+64.2/−12.8	+64.2/−21.4
F2 slits (mm)	+5/−23	+5/−14
F2UD slits (mm)[a]	±3	±3
F2.5 slits (mm)	±100	±100
F2.5UD slits (mm)[a]	±100	±100
F5 slits (mm)	±110	±110
F7 slits (mm)	±15	±15
F7UD slits (mm)[a]	±110	±110
Intensity (pnA)[b]	120	110
Live rate (%)	94	93
Time (h)	40.9	48.7

[a] UD slits are vertical ones. [b] 1 pnA = 6.24×10^9 particles/s.

technique with two clover-type high-purity Ge detectors located downstream of the F7 focal plane. In the experiment, we measured the isomeric decays of ^{94m}Pd and ^{96m}Pd to confirm the PID. A 2-mm Al wedge degrader located at F5 was used for further isotope separation in the second stage.

The experimental settings are presented in Table 1. The $B\rho$ value of the first dipole magnet was 5.320 Tm, which was tuned to maximize the yield of the central particle, i.e. the fully stripped $^{100}Sn^{50+}$ ion. The dipoles downstream were tuned to set the central particle on the beam axis. Two slit settings were employed to optimize the total rate of the RI beams and purity of the RIs of interest in the decay measurement, which was conducted simultaneously as our new-isotope search.

It is essential for the discovery of new isotopes to remove background events inconsistent with the properties of the projectile fragments. Reaction and scattering events in the PID detectors or the F5 degrader, pile-up events, or improper responses of the detectors were rejected by investigating the various correlation plots of the signal timings, pulse heights, beam-spot images, and phase spaces. Additionally, we removed the reaction and charge-changing events at the F5 degrader as well as the pile-up events, by comparing the Z value obtained from the ΔE value measured using the MUSIC at F7 and Z_{F5} deduced from the energy loss in the F5 degrader which was calculated from the magnetic rigidities and velocities in F3–F5 and F5–F7. For further details on the background removal at BigRIPS, see Refs. [34,37,57].

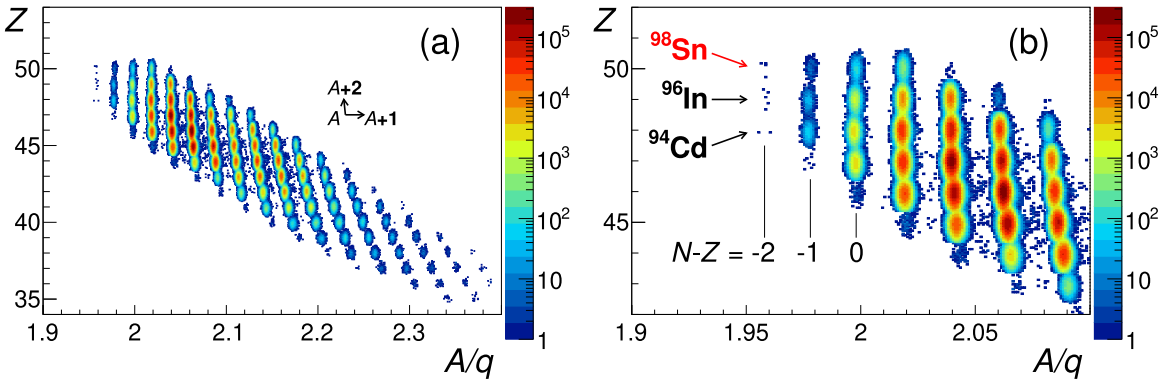

Fig. 2. Z versus A/q PID plots for the highly proton-rich RIs including ^{98}Sn produced in the ^{124}Xe + Be reaction at 345 MeV/nucleon. (a) PID plots for all areas. The arrows show the relation among the mass numbers of the isotopes. The mass numbers of the right and upper-left isotopes are A+1 and A+2, respectively. (b) Enlarged PID plots around the new isotope, ^{98}Sn.

3. Results and discussion

Figure 2 shows the Z versus A/q PID plots. The $B\rho$ values were the same in the two settings, and the obtained PID plots were added. Four ^{98}Sn events were observed. Additionally, we have confirmed the discovery of ^{96}In and ^{94}Cd through the observation of five and two events, respectively. These isotopes were initially identified with two and three events, respectively, in the previous experiment [6] conducted at RIBF.

The A/q resolution was approximately 0.0011 (0.056%), leading to sufficient separation of the adjacent isotopes, as shown in Fig. 2(b). Conversely, the resolution of Z was 0.2, resulting in a 5σ separation. The loci of the adjacent isodiapheres (same neutron excess) overlapped because their A/q values in the $A/q = 2$ region were almost the same. To ensure no leakage events to ^{98}Sn from the neighboring RIs, especially from ^{96}In, we plotted the horizontal position at F3 (F3X) of the $N-Z = -2$, -1, and 0 isodiapheric chains in Fig. 3. The F3X values of the RIs produced at the F0 target can be described by a function of their Z and N values because the RIs were separated based on these values by the $B\rho$-ΔE-$B\rho$ method in the first stage. A larger F3X value is obtained from a smaller Z isodiaphere in each plot in Fig. 3. In every isotopic chain, a smaller N isotope results in a larger F3X value. Around ^{100}Sn, the experimental F3X values were described using Z and N of the RIs as follows:

$$\mathrm{F3X\,[mm]} = 0.8 + 1.3 \times (50 - Z) + 5.9 \times (50 - N). \quad (1)$$

This obtained equation agrees with the F3X values calculated from the ion optics of the separator and the energy loss at the F1 degrader. Figure 3(a) shows that three of the four events at ^{98}Sn in the Z versus A/q plots were located in the F3X systematics shown by the pink line; thus, we concluded that the new isotope of ^{98}Sn was surely observed. The remaining one event was located at $Z = 49.73$ and F3X = 9.1 mm, which is 2.1σ apart from the expected positions of Z = 50.00 and F3X = 12.6 mm, considering the Z and F3X distribution widths. The possibility that this event corresponds to other RIs was investigated, and rejected considering the following. (1) We excluded the possibility of leakage from ^{96}In: Fig. 3(a) shows that the expected F3X value of ^{96}In is larger than that of ^{98}Sn, and the single event is located 6.6σ apart from the expected position of ^{96}In together with the Z separation. (2) The possibility of leakage from ^{99}Sn was rejected: approximately 17σ separation was achieved in A/q. Therefore, we concluded that the single event was also corresponding to ^{98}Sn. The events of ^{94}Cd look not to be located

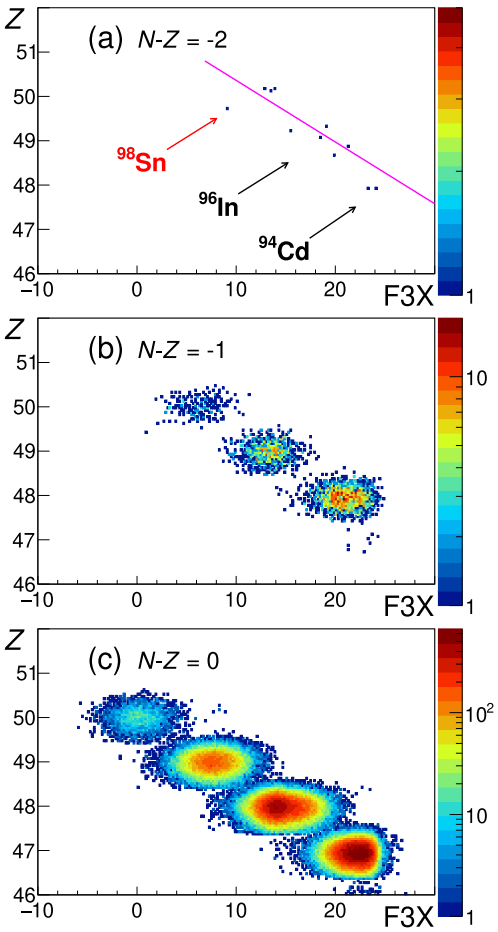

Fig. 3. Z versus F3X plots for the isodiapheric chains with (a) $N-Z=-2$, (b) $N-Z=-1$, and (c) $N-Z=0$. Smaller Z nuclide results in larger F3X in each isodiapheric chain and smaller N nuclide results in larger F3X in each isotopic chain. The pink line shows the F3X systematics for $N-Z=-2$ isodiapheres deduced from the neighboring nuclei. Three ^{98}Sn events were located in the systematics; thus, this nuclide was confirmed as a new isotope. The remaining one event was also concluded to be ^{98}Sn. See text.

in the systematics. This is caused by the F2-slit position of -23 mm, corresponding to $+23$ mm in F3X. Most of the ^{94}Cd nuclei were cut by the F2 slit.

The cross sections of the central particle of ^{100}Sn and its neighboring RIs were deduced from their yields and transmissions in the BigRIPS, which were calculated using the LISE^{++} simulation [58]. In the simulation, we adopted the default parameters of LISE^{++} for the transverse momentum distributions of the RIs. On the contrary, we assumed asymmetric Gaussian distributions for the longitudinal momentums based on the recent ^{78}Kr primary-beam study [46]. We employed the original Goldhaber model [59] for the standard deviation of the high-momentum side σ_0 and 1.1 times the high-momentum one for the low-momentum side, respectively. The cross sections of RIs whose transmission in BigRIPS was less than 10% were not derived, because smaller transmission would result in larger systematic errors in the cross sections. The calculated cross sections change along with the switching of the momentum distribution in the LISE^{++} simulation from the global parameterization [58,60], the default one, to the asymmetric Gaussian, since the momentum distributions are different in these two models. The change in derived cross sections is less than a few percent for well-transmitted (>50%) RIs; however, for low-transmission RIs whose distribution tails were transported, the system-

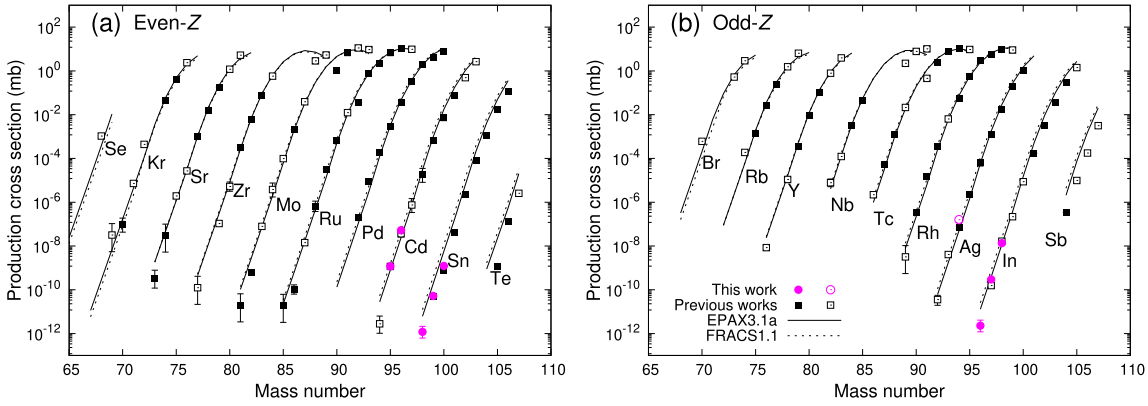

Fig. 4. Measured cross sections of the proton-rich RIs produced in the reaction of ^{124}Xe + Be at 345 MeV/nucleon along with the prediction values of semi-empirical cross-section formulas. (a) Results for even-Z RIs. (b) Results for odd-Z RIs. The pink circles indicate the data obtained in this study, and the black squares indicate previously obtained data. The filled symbols indicate that the distribution peaks of the RIs were located inside the slit opening at each focal plane. The open symbols indicate that the peaks were located outside the slit openings at several focal planes. The lines show the predicted values by the EPAX3.1a and FRACS1.1 cross-section formulas.

atic errors can be significant, and we prefer not to quote them. The cross sections also include systematic errors originating from calibration of the primary-beam intensity. In the derivation of the cross sections of RI beams produced by the ^{78}Kr + Be reaction at BigRIPS [46], the systematic error was assumed to be ±20% from the fluctuation of cross sections of a single RI measured by multiple settings. Similar systematic error is expected in this study. Note that the half-lives of the proton-rich RIs in this study were assumed to be longer than the γ-corrected TOF in the BigRIPS (∼350 ns).

Figure 4 shows the cross sections of the RIs produced in the reaction of 345-MeV/nucleon ^{124}Xe + Be at RIBF, along with predicted values by the EPAX3.1a [61] and FRACS1.1 [62] semi-empirical formulas. The pink circles and black squares show the cross sections obtained in this study and those evaluated in Ref. [63] using the data from previous studies [6,14,38,39], respectively. The filled symbols indicate that the distribution peaks of the RIs were located inside the slit opening at each focal plane. The transmissions of these RIs were typically greater than 30% including the charge distribution in the Z region of ∼50 and energy region of ∼200 MeV/u in our study. The open symbols indicate that the peaks were located outside the slit openings at several focal planes. The cross sections obtained in this study were consistent with the previous data obtained at RIBF. The cross sections of ^{98}Sn, ^{99}Sn, and ^{100}Sn are $(1.20^{+0.95}_{-0.57})\times10^{-12}$ mb, $(5.23\pm0.71)\times10^{-11}$ mb, and $(1.23\pm0.05)\times10^{-9}$ mb, respectively; and they are, respectively, 1/5.1, 1/3.6, and 1/4.7 of the values predicted by EPAX3.1a. Overall, the discrepancy between the experimental cross sections and the EPAX3.1a predictions increases in the more exotic region and closer-Z region to the projectile. This trend was also observed in the production of proton-rich RI beams from the 345-MeV/nucleon ^{78}Kr beam [46].

On the proton-rich side, some nucleon-unbound RIs have long half-lives (>1 ms) for proton emission due to the need to tunnel through the Coulomb and centrifugal barriers; thus, observing these RIs does not directly mean that they are bound. In some cases, the yields of RIs were much smaller than the yield systematics of their neighboring RIs, such as odd-Z $^{68}_{35}$Br [41,46], $^{89}_{45}$Rh [6], and $^{93}_{47}$Ag [6]. For these isotopes, the suggested half-life upper limits of ∼100 ns indi-

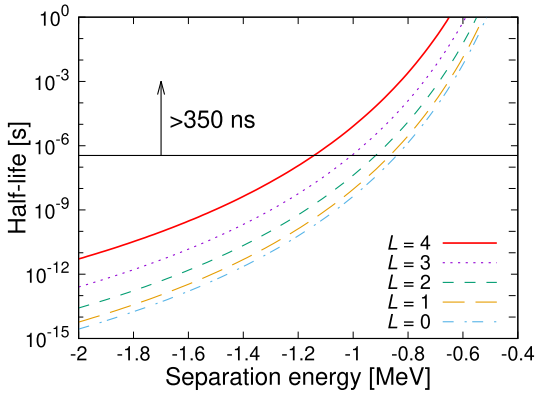

Fig. 5. Half-life of ^{96}In calculated using the empirical equation in Ref. [64]. $L = 4$ is the most probable angular momentum transfer because the emitted proton is located at $1g_{9/2}$ assuming that ^{96}In is spherical.

cated that they are proton unbound. However, only a few events of the isodiapheres with $N-Z = -2$ were identified in this study; thus, we could not determine whether they are bound or not.

Most of the mass models predict that ^{98}Sn is bound: a shell-model calculation in the $2p_{3/2}$, $1f_{5/2}$, $2p_{1/2}$, and $1g_{9/2}$ shells [16], the empirical mass formula KTUY [18], the finite-range droplet formula FRDM12 [19], the Weizsäcker-Skyrme microscopic-macroscopic mass formula WS4$_{\rm RBF}$ [20], a version of the nonrelativistic Hartree–Fock–Bogoliubov models (HFB14) [21], and two energy-density functional models based on UNEDF0 [25] and UNEDF1 [26]. Another shell-model calculation in the $2p_{1/2}$ and $1g_{9/2}$ shells [17], WS4 [20], and HFB32 [24] predict that this nuclide is a $2p$ emitter. It is predicted to be unbound by HFB21 [22] and HFB24 [23]. There are no values given in the AME2016 [27] and AME2020 [15] mass tables.

The abovementioned models predict that the lower-Z isodiapheres are also located around the boundary between proton-bound and unbound nature. All models except KTUY or HFB24 predict that the other even-Z isodiaphere ^{94}Cd is bound. It is predicted to be a $2p$ emitter by KTUY and HFB24. The degree of boundness of ^{98}Sn and ^{94}Cd depends on the models.

All the mass models predict that the odd-Z isodiaphere of ^{96}In is unbound: its proton separation energy (S_p) ranges from -1.68 to -0.13 MeV. The half-life of ^{96}In was not directly measured in our study; however, it is considered to be longer than the γ-corrected TOF of $\sim$350 ns. If its half-life is shorter than 350 ns, the apparent cross section should look smaller owing to its in-flight decay. However, no significant reduction of ^{96}In was observed compared with the even-Z isodiapheres, ^{98}Sn and ^{94}Cd, as shown in Fig. 4. Therefore, our assumption that the half-life of ^{96}In is longer than 350 ns is reasonable. The S_p value of ^{96}In was estimated using the empirical equations between the half-lives and S_p [64,65]. Figure 5 shows the half-life calculated using the equation in Ref. [64] as a function of S_p for each angular momentum transfer L. ^{96}In is expected to be spherical, because it is close to the double-magic nuclide ^{100}Sn. Considering that the emitted proton is likely to occupy the $1g_{9/2}$ orbital, $L = 4$ is most reasonable. Therefore, we evaluated the S_p value to be greater than -1.14 MeV from the lower limit of the half-life, 350 ns. The empirical equation in Ref. [65] provides a similar value of -1.13 MeV. The FRDM12, UNEDF0, UNEDF1, HFB14, and HFB32 mass models predict an S_p value of greater than -1.1 MeV. HFB32 predicts the largest S_p value of -0.13 MeV; the proton-emission half-life is estimated to be longer than 1 s by the empirical equations. On the other

hand, the β-decay half-life of ^{96}In is expected to be on the order of ms, because the β-decay half-life of the one-less neutron-deficient RI of ^{97}In is 36 ms [66]. Therefore, the decay of ^{96}In could be a competition between the proton emission and β decay, or even β decay only.

Measuring the decay mode and half-life of ^{96}In is essential to understand the contribution of this nuclide to the *rp*-process whose paths are around the proton dripline [9,10]. ^{96}In might work as a path if the half-life of the proton emission is comparable to that of the β decay. To determine the half-life, measuring the in-flight decay using 2-fold PID sections or decay of the nuclide injected into some detectors is required.

4. Summary

We discovered a new isotope of ^{98}Sn produced by a reaction of ^{124}Xe + Be at 345 MeV/nucleon at RIBF, RIKEN. Additionally, we reverified the previously discovered new isotopes at RIKEN, ^{96}In and ^{94}Cd. The highly proton-rich RIs, including ^{98}Sn, were separated and identified using the in-flight separator BigRIPS. The cross section of ^{98}Sn was $(1.20^{+0.95}_{-0.57})\times10^{-12}$ mb corresponding to 1/5.1 of the prediction value of the semi-empirical formula EPAX3.1a. The boundness of ^{98}Sn could not be determined from our measurements; however, most of the mass models predict that it is bound. On the other hand, ^{96}In is predicted to be unbound. Since no significant yield reduction of ^{96}In was observed compared with the adjacent even-Z isodiapheres, its half-life was assumed to be longer than 350 ns, which was the γ-corrected TOF value in BigRIPS. Since some mass models predict a long half-life (>1 s) of proton emission, there is a possibility that the decay of ^{96}In may exhibit competition between the proton emission and β decay.

Acknowledgements

This study was conducted at the RI Beam Factory operated by the RIKEN Nishina Center, RIKEN, and Center for Nuclear Study, University of Tokyo. The authors are grateful to the RIBF accelerator team for supplying the stable beam of ^{124}Xe.

Funding

This work was partially supported by the Spanish grants of Ministry of Economy and Competitiveness (MINECO) FPA2014-52823-C2-1-P, MICINN/AEI FPA2017-83946-C2-1-P, MICINN/AEI PID2019-104714GB-C21, and PID2022-138297NB-C21, Japan Society for the Promotion of Science (JSPS) Invitational Fellowships for Research in Japan (ID: L1955), the Prometeo excellence programme of the Generalitat Valenciana (CIPROM/2022/9 and ASFAE/2022/027), NKFIH (K147010), and the U.S. Department of Energy (DOE) under the contract DE-AC05-00OR22725 (ORNL).

References

[1] D. E. M. Hoff et al., Nature **580**, 52 (2020).
[2] K. Wimmer et al., Phys. Rev. Lett. **126**, 072501 (2021).
[3] M. Lewitowicz et al., Phys. Lett. B **332**, 20 (1994).
[4] R. Schneider et al., Z. Phys. A **348**, 241 (1994).
[5] C. B. Hinke et al., Nature **486**, 341 (2012).
[6] I. Čeliković et al., Phys. Rev. Lett. **116**, 162501 (2016).
[7] J. Park et al., Phys. Rev. C **99**, 034313 (2019).
[8] M. Gorska, Physics **2022**, 364 (2022).

[9] H. Schatz, A. Aprahamian, V. Barnard, L. Bildsten, A. Cumming, M. Ouellette, T. Rauscher, F.-K. Thielemann, and M. Wiescher, Phys. Rev. Lett. **86**, 3471 (2001).
[10] S. Wanajo, H.-T. Janka, and S. Kubono, Astrophys. J. **729**, 46 (2011).
[11] R. E. Taam, Astrophys. J. **241**, 358 (1980).
[12] O. Koike, M. Hashimoto, R. Kuromizu, and S. Fujimoto, Astrophys. J. **603**, 242 (2004).
[13] Z. Janas et al., Phys. Rev. Lett. **82**, 295 (1999).
[14] H. Suzuki et al., Phys. Rev. C **96**, 034604 (2017).
[15] M. Wang, W. J. Huang, F. G. Kondev, G. Audi, and S. Naimi, Chin. Phys. C **45**, 030003 (2021).
[16] R. Tian, H. Li, Y. Hu, and C. Dong, Res. Phys. **33**, 105173 (2022).
[17] H. Herndl and B. A. Brown, Nucl. Phys. A **627**, 35 (1997).
[18] H. Koura, T. Tachibana, M. Uno, and M. Yamada, Prog. Theor. Phys. **113**, 305 (2005).
[19] P. Möller, W. D. Myers, H. Sagawa, and S. Yoshida, Phys. Rev. Lett. **108**, 052501 (2012).
[20] N. Wang, M. Liu, X. Wu, and J. Meng, Phys. Lett. B **734**, 215 (2014).
[21] S. Goriely, M. Samyn, and J. M. Pearson, Phys. Rev. C **75**, 064312 (2007).
[22] S. Goriely, N. Chamel, and J. M. Pearson, Phys. Rev. C **82**, 035804 (2010).
[23] S. Goriely, N. Chamel, and J. M. Pearson, Phys. Rev. C **88**, 024308 (2013).
[24] S. Goriely, N. Chamel, and J. M. Pearson, Phys. Rev. C **93**, 034337 (2016).
[25] M. Kortelainen, T. Lesinski, J. Moré, W. Nazarewicz, J. Sarich, N. Schunck, M. V. Stoitsov, and S. Wild, Phys. Rev. C **82**, 024313 (2010).
[26] M. Kortelainen, J. McDonnell, W. Nazarewicz, P.-G. Reinhard, J. Sarich, N. Schunck, M. V. Stoitsov, and S. M. Wild, Phys. Rev. C **85**, 024304 (2012).
[27] M. Wang, G. Audi, F. G. Kondev, W. J. Huang, S. Naimi, and X. Xing, Chin. Phys. C **41**, 030003 (2017).
[28] Y. Yano, Nucl. Instrum. Methods Phys. Res. B **261**, 1009 (2007).
[29] Y. Shimizu et al., Nucl. Instrum. Methods Phys. Res. B **463**, 158 (2020).
[30] Y. Shimizu et al., RI-Beam Yield Database webpage. https://ribeam.riken.jp.
[31] T. Ohnishi et al., J. Phys. Soc. Jpn. **77**, 083201 (2008).
[32] T. Ohnishi et al., J. Phys. Soc. Jpn. **79**, 073201 (2010).
[33] T. Sumikama et al., Phys. Rev. C **95**, 051601 (2017).
[34] N. Fukuda et al., J. Phys. Soc. Jpn. **87**, 014202 (2018).
[35] Y. Shimizu et al., J. Phys. Soc. Jpn. **87**, 014203 (2018).
[36] T. Sumikama et al., Phys. Rev. C **103**, 014614 (2021).
[37] Y. Shimizu et al., Phys. Rev. C **109**, 044313 (2024).
[38] H. Suzuki et al., Nucl. Instrum. Methods Phys. Res. B **317**, 756 (2013).
[39] H. Suzuki et al., Phys. Rev. Lett. **119**, 192503 (2017).
[40] B. Blank et al., Phys. Rev. C **93**, 061301(R) (2016).
[41] K. Wimmer et al., Phys. Lett. B **795**, 266 (2019).
[42] O. B. Tarasov et al., Phys. Rev. Lett. **121**, 022501 (2018).
[43] M. Yoshimoto et al., Prog. Theor. Exp. Phys. **2024**, 101D01 (2024).
[44] D. S. Ahn et al., Phys. Rev. Lett. **129**, 212502 (2022).
[45] R. Serber, Phys. Rev. **72**, 1114 (1947).
[46] H. Suzuki et al., Prog. Theor. Exp. Phys., submitted, https://doi.org/10.1093/ptep/ptaf050.
[47] O. B. Tarasov, Abrasion-Ablation model webpage. https://lise.nscl.msu.edu/AA.
[48] T. Kubo, Nucl. Instrum. Methods Phys. Res. B **204**, 97 (2003).
[49] T. Kubo et al., IEEE. Appl. Supercond. **17**, 1069 (2007).
[50] T. Kubo et al., Prog. Theor. Exp. Phys. **2012**, 03C003 (2012).
[51] J. P. Dufour, R. Del Moral, H. Emmermann, F. Hubert, D. Jean, C. Poinot, M. S. Pravikoff, A. Fleury, H. Delagrange, and K.-H. Schmidt, Nucl. Instrum. Methods Phys. Res. A **248**, 267 (1986).
[52] K.-H. Schmidt, E. Hanelt, H. Geissel, G. Münzenberg, and J. P. Dufour, Nucl. Instrum. Methods Phys. Res. A **260**, 287 (1987).
[53] D. S. Ahn, H. Suzuki, N. Fukuda, Y. Shimizu, H. Takeda, K. Yoshida, Y. Yanagisawa, N. Inabe, and T. Kubo, RIKEN Accel. Prog. Rep. **52**, 133 (2019).
[54] H. Kumagai, T. Ohnishi, N. Fukuda, H. Takeda, D. Kameda, N. Inabe, K. Yoshida, and T. Kubo, Nucl. Instrum. Methods Phys. Res. B **317**, 717 (2013).
[55] K. Kimura et al., Nucl. Instrum. Methods Phys. Res. A **538**, 608 (2005).
[56] Y. Sato et al., Jpn. J. Appl. Phys. **53**, 016401 (2014).

[57] N. Fukuda, T. Kubo, T. Ohnishi, N. Inabe, H. Takeda, D. Kameda, and H. Suzuki, Nucl. Instrum. Methods Phys. Res. B **317**, 323 (2013).
[58] O. B. Tarasov and D. Bazin, Nucl. Instrum. Methods Phys. Res. B **266**, 4657 (2008), and references therein; LISE^{++} web page, https://lise.nscl.msu.edu .
[59] A. S. Goldhaber, Phys. Lett. **53B**, 306 (1974).
[60] O. B. Tarasov, Nucl. Phys. A **734**, 536 (2004).
[61] K. Sümmerer, Phys. Rev. C **86**, 014601 (2012).
[62] B. Mei, Phys. Rev. C **95**, 034608 (2017).
[63] BigRIPS RI-beam Intensity web page, https://www.nishina.riken.jp/RIBF/BigRIPS/intensity.html.
[64] C. Qi, D. S. Delion, R. J. Liotta, and R. Wyss, Phys. Rev. C **85**, 011303(R) (2012).
[65] J.-L. Chen, J.-Y. Xu, J.-G. Deng, X.-H. Li, B. He, and P.-C. Chu, Eur. Phys. J. A **55**, 214 (2019).
[66] J. Park et al., Phys. Rev. C **97**, 051301(R) (2018).